# Interfacial Depth Profiling of the Orientation and Bonding of Water Molecules across Liquid−Liquid Interfaces

**Dave S. Walker[†] and Geraldine L. Richmond***

*Department of Chemistry and Materials Science Institute, University of Oregon, Eugene, Oregon 97403*

*Received: July 12, 2007; In Final Form: September 21, 2007*

Molecular interactions that create the interfacial properties present at a junction between water and several hydrophobic liquids are the focus of this paper. This study employs molecular dynamics simulations to generate vibrational sum frequency (VSF) spectral profiles of water across the interfacial depth of three systems: the carbon tetrachloride−water, chloroform−water, and dichloromethane−water interfaces. These spectral profiles are calculated as functions of both frequency and interfacial depth, providing a visual description of interfacial water structure that can be difficult to elucidate from density profiles and sum frequency spectral intensities, or spectra that vary only as functions of frequency. VSF spectral intensities calculated for the OH stretch region that are integrated over the entire interfacial region are shown to compare well with the experimental VSF data for these systems. VSF spectral depth profiles show how the widths of the interfaces vary with the density and polarity of the organic phase and where different types of water species reside in the interfacial region. Furthermore they highlight the major molecular level differences found in these three interfacial regions and, in particular, identify oriented water monomers deeply immersed within the dichloromethane phase far removed from the Gibbs dividing surface. The penetration of water has important implications for how we view transport across water−hydrophobic liquid interfaces.

## Introduction

The interface between water and a hydrophobic liquid is the site for many important processes that are utilized for biological, environmental, and industrial applications. The carbon tetrachloride−water ($CCl_4$−$H_2O$), chloroform−water ($CHCl_3$−$H_2O$), and dichloromethane−water ($CH_2Cl_2$−$H_2O$) interfaces serve as a series of model systems that are studied on a frequent basis due to their fundamental and simple nature, both experimentally and computationally. The organic molecules themselves comprise the simplest type of halocarbon, yet each molecule possesses unique physical properties that enable clear distinction between them. Their spectroscopic response within the vibrational OH stretch region of water is nearly transparent, making them ideal candidates for spectroscopic studies of water−hydrophobic surfaces. As a result, there is considerable interest in understanding the structural properties of water within these buried systems, especially by means of vibrational spectroscopy.[1−10]

Whereas both linear and nonlinear vibrational spectroscopic techniques have been shown to be powerful methods for studying the surface of water on a molecular level, understanding the nature of the water surface on the basis of its spectral response poses many challenges. The surface is comprised of a multitude of hydrogen-bonded water species of different bond lengths, strengths, and angles, making it nearly impossible to assign distinct frequencies and bandwidths to particular types of hydrogen-bonded water molecules as has been possible for gas-phase water and its simple clusters. Furthermore, current analytical approaches toward understanding the vibrational spectroscopic response of liquid surfaces cannot provide direct information pertaining to the location of different contributing species within the interfacial region. Experimentally, techniques such as X-ray scattering,[11−13] neutron scattering,[14,15] and second harmonic studies[16,17] assist in our understanding of interfacial structure as a function of depth, but they cannot capture the molecular bonding nature of these interfacial water species that VSF studies can provide.

On a computational level, density profiles are common tools that are used to assess interfacial thickness, by correlating the interfacial region to changes in the molecular population of a given liquid.[1,8,18−22] In this work, molecular dynamics simulations are used to create spectral profiles of water at the $CCl_4$−$H_2O$ interface, the $CHCl_3$−$H_2O$ interface, and the $CH_2Cl_2$−$H_2O$ interface. These spectral profiles combine the methodologies behind vibrational sum frequency spectroscopy and density profiles to create spectral responses of water that vary as functions of both frequency and interfacial depth. By the combination of these two methods, properties such as interfacial depth and penetration of water into the adjacent medium are assessed by observing the molecular orientation of extant water molecules, as opposed to changes in molecular population. To emphasize these changes within the different interfacial systems, several species of water that interact directly with the organic phases are identified, and the spectral profiles from each species are evaluated. These results are compared with measurements obtained from density profiles and sum frequency spectral intensities to show how spectral profiles identify properties of water within the interfacial region that can be particularly difficult to deduce from these other standard treatments. These studies show how differently the interfacial water molecules behave when present at the surface of organic liquids of varying density and polarity.

* To whom correspondence should be addressed. E-mail: Richmond@uoregon.edu. Phone: 541-346-4635. Fax: 541-346-5859.

[†] TriQuint Semiconductor Inc., Hillsboro, OR 97124.

10.1021/jp075469w CCC: $40.75 
Published on Web 12/12/2007

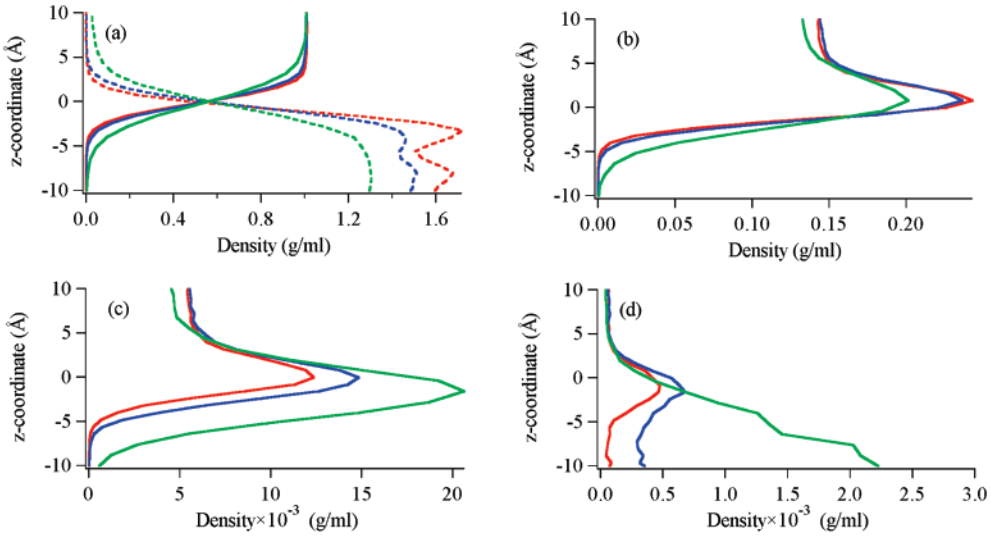


**Figure 1.** Density profiles of (a) water (solid) and organic (dashed) liquids, (b) straddling water molecules, (c) hydrogen bond acceptors, and (d) water monomers at the $CCl_4-H_2O$ (red), $CHCl_3-H_2O$ (blue), and $CH_2Cl_2-H_2O$ (green) interfaces.

## Computational Details

Molecular dynamics simulations of $CCl_4-H_2O$, $CHCl_3-H_2O$, and $CH_2Cl_2-H_2O$ interfaces were performed with the AMBER 7 package using fully atomic, polarizable descriptions for each molecule.[23] Initially, 2135 $H_2O$ molecules,[24] 400 $CCl_4$ molecules,[25] 475 $CHCl_3$ molecules,[26] and 601 $CH_2Cl_2$ molecules[20] were each equilibrated for 200 ps in separate cells measuring 40 Å × 40 Å × 40 Å to produce bulk liquid systems. Following this initial equilibration, liquid−liquid interfacial systems were created by joining together one water cell with one or two organic liquid cells along the *z*-axis to produce systems measuring 40 Å × 40 Å × 80 Å or 40 Å × 40 Å × 120 Å. The $CCl_4-H_2O$ and $CHCl_3-H_2O$ systems sufficed with one organic liquid box. The $CH_2Cl_2-H_2O$ system required a second organic liquid cell to accommodate for the increased solubility of $H_2O$ in $CH_2Cl_2$. The center of the $CH_2Cl_2$ phase was treated as a reservoir for $H_2O$ molecules and was not used for data collection. Consequentially, the same 40 Å × 40 Å × 80 Å region surrounding $H_2O$ was used for data collection in all interfacial systems. Following minimization, all of these systems were equilibrated for 2 ns, followed by data collection over the course of the next 3 ns to produce 60 000 configurations. The time step of integration was 1 fs. The particle mesh Ewald technique applied an 8 Å cutoff toward long-range interactions. All simulations were performed under the NVT scheme at 300 K with weak coupling to a heat bath.

A modified Morita and Hynes frequency-domain treatment[27] was applied to generate sum frequency spectral responses from water in each of these liquid−liquid systems and has been described in detail elsewhere.[28] These modifications included use of a dipole−dipole coupling term to model geometrically favored intermolecular hydrogen bonds in water, a varying intramolecular coupling constant based on the degree of solvation for each water molecule, and a reduced homogeneous broadening term (2 $cm^{-1}$) to enable resolution of narrow peaks in the spectral response for certain species of water. Resolution of narrow peaks could not be attained with the value of the homogeneous broadening used in the original treatment (22 $cm^{-1}$),[27] but can be observed more clearly using smaller values.

In this computational treatment, it is found that the most distinguishing interfacial water molecules for these three liquid−liquid systems fall into three categories. The first species are "straddling" water molecules.[4] This type of water molecule "straddles" the interface and has one OH oscillator directed towards the water phase where it participates as a hydrogen bond donor to another water molecule, and its companion OH oscillator directed towards the organic phase where it does not participate as a hydrogen bond donor to another water molecule. (No distinction is made here for OH oscillators with different degrees of intermolecular hydrogen bonds on the oxygen atom.) These two OH oscillators are energetically uncoupled due to their different environments and are commonly referred to in the literature as the "donor OH mode" and "free OH mode", respectively.[4,5] In this work, the focus of the discussion is largely on the free OH mode, as this mode interacts directly with the organic phase while the donor OH mode does not. Beyond these, the second type of water molecules discussed is hydrogen bond acceptors. These molecules only interact with adjacent water molecules by means of intermolecular hydrogen bonding on their oxygen atoms and possess distinctly different behavior at these three liquid−liquid interfaces. They are found to be highly oriented with their OH oscillators directed toward the bulk organic phase, minimizing their ability to bond as hydrogen bond donors. As is the case with straddling water molecules, separate categories are not made between hydrogen bond acceptors with different degrees of intermolecular hydrogen bonds on the oxygen atom. The third species are water monomers. These molecules possess no intermolecular hydrogen bonds to other water molecules and are largely surrounded by organic molecules. The criterion for hydrogen bonding in this work was an intermolecular OH bond length of 2.5 Å. Although different polarization schemes are straightforward to generate computationally, all calculated spectra in this work are collected in SSP polarization to enable comparison with current experimental measurements.[5,29]

## Results and Discussion

Figures 1a through 1d show density profiles of water, organic liquids, and species of water that interact directly with organic liquids at each liquid−liquid interface. For each figure, the vertical axis represents the *z*-coordinate (which resides perpendicular to the interfacial plane) and the horizontal axis represents the density. Positive values of the *z*-coordinate represent the water phase, negative values of the *z*-coordinate represent the organic phase, and $z = 0$ Å approximates the Gibbs dividing surface.

Figure 1a shows that the density profiles of water at the $CCl_4-H_2O$ and $CHCl_3-H_2O$ interfaces are very similar, while the profile of water at the $CH_2Cl_2-H_2O$ interface is distinctly different with its water population extending deeper into the organic phase. This observation coincides with the increased polarity of $CH_2Cl_2$ compared to both $CCl_4$ and $CHCl_3$ and is indicative of a wider interfacial region. In conjunction with their respective water profiles, Figure 1b shows that the density profile of straddling water molecules also extends deeper into the organic phase at the $CH_2Cl_2-H_2O$ interface than at the other liquid−liquid interfaces. In addition to this wider region of density, straddling water molecules possess a lower peak density at the $CH_2Cl_2-H_2O$ interface (approximately 0.20 g/mL) compared to the other interfaces (approximately 0.25 g/mL). Density profiles of water and straddling water molecules at the $CCl_4-H_2O$ and $CHCl_3-H_2O$ interfaces are similar to their corresponding profiles at the vapor−water interface, indicating a lack of significant perturbation upon the interfacial water population by $CCl_4$ or $CHCl_3$.[28] There is however a clear spectroscopic distinction between straddling water molecules immersed within different interfacial systems as indicated by a shift in the calculated vibrational frequency of the free OH mode (of which the liquid−liquid results are to be discussed below), consistent with experimental results.[4,5,30,31]

Figure 1c shows that the interfacial location of peak populations and the degrees of penetration into the organic phase from hydrogen bond acceptors are directly related to the polarity of each organic liquid: the greater the permanent dipole moment of the organic liquid, the greater the peak population and overall quantity of hydrogen bond acceptors that penetrate into the organic phase. This trend is seen in a more dramatic fashion in Figure 1d for water monomers. But unlike hydrogen bond acceptors, not all density profiles for water monomers possess peak populations at the interface. The density profile of water monomers at the $CH_2Cl_2-H_2O$ interface continues to increase in population more than 10 Å away from the Gibbs surface. Within the $CH_2Cl_2$ phase, the density of water reasonably reproduces the estimated solubility of water in $CH_2Cl_2$ (between $2 \times 10^{-3}$ and $3 \times 10^{-3}$ g/mL). The density profiles of water monomers at the $CCl_4-H_2O$ and $CHCl_3-H_2O$ interfaces relatively possess peak populations at the interface and undergo a relatively steady decrease in population as a function of depth within the organic phase.

It should be noted that Figure 1a shows the organic liquids at the $CCl_4-H_2O$ and $CHCl_3-H_2O$ interfaces possess additional interfacial structure not seen in the case of the $CH_2Cl_2-H_2O$ interface, as manifested in the oscillatory behavior of their density profiles. The molecular structure of $CCl_4$ at the $CCl_4-H_2O$ interface has been explored in previous studies, with the oscillations observed at that interface attributed to a layered, oriented packing of $CCl_4$ molecules.[32] The composition of the $CHCl_3-H_2O$ interface has also been studied,[33] with the oscillation in density observed for $CHCl_3$ molecules to be indicative of a lesser degree of oriented packing from those molecules. In contrast, the density profile of $CH_2Cl_2$ molecules undergoes a smooth transition from the organic phase to the water phase, indicating a lack of layered packing from those molecules.

Finally, the bulk water population approaches its corresponding bulk density, yet Figures 1b and 1c show that the hydrogen bond acceptor population and the free OH population do not converge onto the same density for all systems within the interfacial depths shown. This is attributed to $CH_2Cl_2$ molecules that penetrate deeper into the water phase compared to $CCl_4$ molecules or $CHCl_3$ molecules, and also attributes to the increased interfacial thickness of the $CH_2Cl_2-H_2O$ system. In essence, the water population approaches its bulk composition, yet continues to feel the presence of the organic liquid surface. The average number of hydrogen bonds within this region is approximately 3.2 bonds per molecule, on the low end of the hydrogen-bonding scale commonly observed in simulations of bulk water.[34]

Figures 2a through 2c show sum frequency spectral depth profiles in SSP polarization of water at the $CCl_4-H_2O$, $CHCl_3-H_2O$, and $CH_2Cl_2-H_2O$ interfaces, respectively. The vertical axes of Figures 2a through 2c represent the z-coordinate, and their horizontal axes represent infrared (IR) frequency within the vibrational OH stretch region. For these figures, as is the case for Figure 1, positive z-coordinate values represent the water phase, and negative z-coordinate values represent the organic phase. By simple inspection it is clear that the $CH_2Cl_2-H_2O$ interface is broader and quite different in the bonding distribution of $H_2O$ when compared to the $CCl_4-H_2O$ and $CHCl_3-H_2O$ interfaces. This is manifested in the bright regions extending deeper into both the organic phase and the water phase. Figure 2d shows the corresponding VSF spectral intensities calculated for these three systems when their spectral profiles are integrated over the z-coordinate. The general features of the spectral intensities for the $CCl_4-H_2O$ and $CHCl_3-H_2O$ interfaces correlate well with experimental measurements.[5,29]

Figure 2a representing the sum frequency spectral depth profile of the $CCl_4-H_2O$ interface displays two distinct features: a sharp peak of high intensity at high frequencies and a relatively narrow region of lower spectral intensity that spans several hundred wavenumbers at lower frequencies. With respect to the sum frequency spectral intensity of the $CCl_4-H_2O$ interface shown in Figure 2d, the sharp peak is commonly associated with the free OH mode, and the broad spectral region is commonly associated with a combination of donor OH modes and fully solvated water molecules.[1,5,8] Figure 2b corresponding to the sum frequency spectral profile of the $CHCl_3-H_2O$ interface displays similar characteristics with respect to those of the $CCl_4-H_2O$ interface, except over a slightly wider interfacial region. This observation is discernible from Figure 1a, where the interfacial width of the $CHCl_3-H_2O$ interface is shown to be slightly broader than the interfacial width of the $CCl_4-H_2O$ interface. Figure 2d shows that the sum frequency spectral intensity of the $CHCl_3-H_2O$ interface is also very similar to that of the $CCl_4-H_2O$ interface. By means of both computational and experimental deconvolution, the spectral peaks associated with the free OH mode at the $CCl_4-H_2O$ and $CHCl_3-H_2O$ interfaces are generally shifted toward lower frequencies by approximately 30 $cm^{-1}$ when compared to the corresponding peak at the vapor−water interface.[4,5,30,31]

It should be noted that Figures 2a and 2b reveal potential limitations in the ability to attain quantitative information regarding the spectral widths of narrow features, e.g., the free OH mode. The exchange time scales of water molecules between interfacial layers are suspected to be of comparable magnitude to the dephasing time of the free OH peak—on the order of 1−10 ps. The effect of this relationship will manifest itself in a broadening of the peak as a function of interfacial depth. When this is combined with the fact that motional narrowing is also not considered in this computational treatment,[28] the overall consequence is a broadening of spectral features, as functions of both frequency and interfacial depth, resulting in only qualitative validity when comparing the narrow features for these interfacial systems.

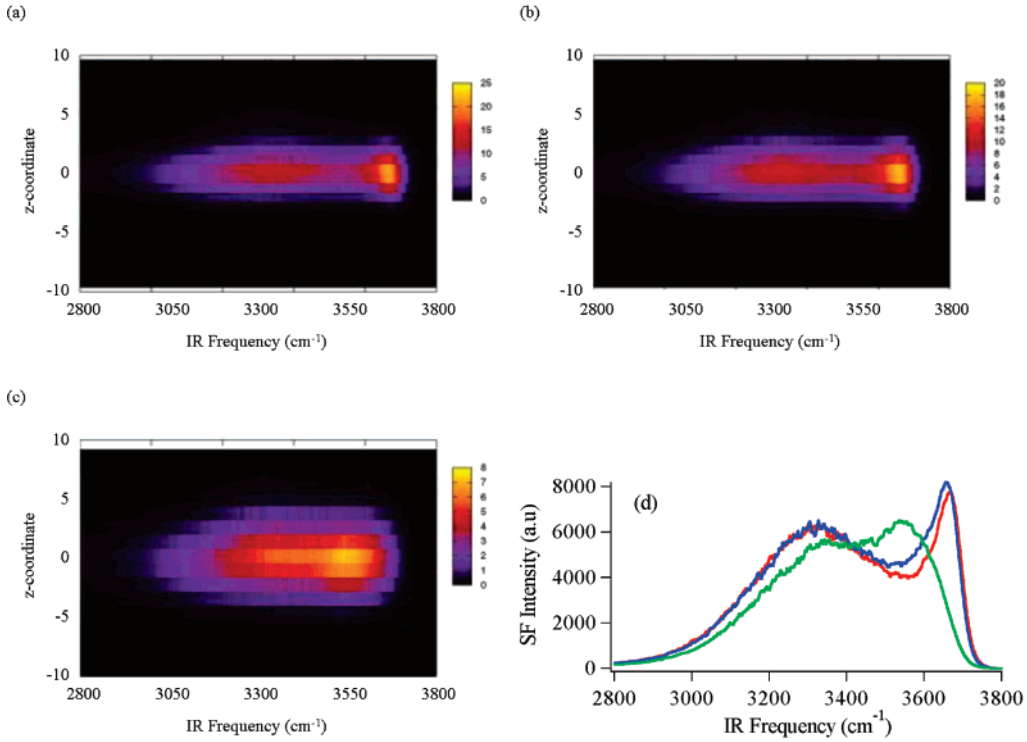


**Figure 2.** Sum frequency spectral profiles of water at the (a) $CCl_4-H_2O$ interface, (b) $CHCl_3-H_2O$ interface, and (c) $CH_2Cl_2-H_2O$ interface. (d) Sum frequency spectral intensities of water at the $CCl_4-H_2O$ (red), $CHCl_3-H_2O$ (blue), and $CH_2Cl_2-H_2O$ (green) interfaces. All spectra are shown in SSP polarization and possess bin sizes of 1 Å and/or 1 $cm^{-1}$.

Figure 2c shows the sum frequency spectral profile of the $CH_2Cl_2-H_2O$ interface is far broader than the spectral profiles of the $CCl_4-H_2O$ and $CHCl_3-H_2O$ interfaces. In addition, the location of two distinct spectral regions is more difficult to identify in either the spectral profile or spectral intensity (Figure 2d) of the $CH_2Cl_2-H_2O$ interface. This "featureless" type of spectral response by water has been observed previously at the 1,2-dichloroethane−water (DCE−$H_2O$) interface.[7,8] In that system, the sum frequency response associated with the free OH mode is not clearly distinguishable due to strong $H_2O$−DCE interactions that result in spectral interferences between straddling water molecules and hydrogen bond acceptors. Efforts to measure experimentally the VSF spectrum of water at the $CH_2Cl_2-H_2O$ interface have not been successful due to the higher adsorptive nature and lower boiling point of $CH_2Cl_2$. However, experimental studies of $CCl_4-H_2O$ interfaces mixed with increasing concentrations of $CH_2Cl_2$ within the $CCl_4$ phase show similar trends as were observed with related concentration studies of DCE added to $CCl_4$.[35] As the $CH_2Cl_2$ concentration is increased in the $CCl_4$ phase there is a progressive loss in spectral intensity, apparent red shift, and spectral broadening of the free OH mode. These experimental observations are consistent with the more featureless spectral response found in these calculations. Understanding the source of these observations is part of the focus of this study.

The data in Figures 3−6 illustrate the spectral contributions as a function of interfacial depth from the three types of interfacial water molecules discussed above. Figures 3a through 3c describe sum frequency spectral profiles of the free OH mode from straddling water molecules at the $CCl_4-H_2O$, $CHCl_3-H_2O$, and $CH_2Cl_2-H_2O$ interfaces, respectively. Figure 3d shows their corresponding calculated sum frequency intensities. All of these spectra are shown in SSP polarization. Figures 3a and 3b show the spectral profiles of the free OH modes at the $CCl_4-H_2O$ and $CHCl_3-H_2O$ interfaces are quite similar in both overall shape and magnitude. The spectral profile of the free OH mode at the $CHCl_3-H_2O$ interface is slightly broader, both in frequency and interfacial depth, and possesses lower peak intensity than the corresponding profile at the $CCl_4-H_2O$ interface. Figure 3d shows that these differences observed in their spectral profiles result in a contributing sum frequency spectral intensity that is slightly greater for the free OH mode at the $CHCl_3-H_2O$ interface than at the $CCl_4-H_2O$ interface. In addition, the free OH mode at the $CHCl_3-H_2O$ interface is shifted slightly to lower frequencies compared to that of the $CCl_4-H_2O$ interface, representative of slightly stronger $H_2O-CHCl_3$ interactions compared to $H_2O-CCl_4$ interactions. Overall, these two peaks are responsible for the sharp features observed in the total spectral responses of water that reside at higher vibrational frequencies for these systems (see Figures 2a, 2b, and 2d).

Figure 3c shows the spectral depth profile of the free OH mode at the $CH_2Cl_2-H_2O$ interface is noticeably different from those of the $CCl_4-H_2O$ and $CHCl_3-H_2O$ interfaces. The free OH mode at the $CH_2Cl_2-H_2O$ interface is very broad both in frequency and interfacial depth. In addition to its spectral depth profile, Figure 3d shows that the calculated sum frequency spectral intensity of the free OH mode at the $CH_2Cl_2-H_2O$ interface is significantly shifted toward lower frequencies compared to those of the other interfaces due to strong $H_2O-CH_2Cl_2$ interactions. However, unlike the free OH peaks observed from these other interfacial systems, the free OH peak observed for the $CH_2Cl_2-H_2O$ interface is not clearly distinguishable within the total spectral response of water (see Figures 2c and 2d): This free OH mode possesses a peak well above 3600 $cm^{-1}$, yet there is no peak above 3600 $cm^{-1}$ observed in the total spectral response of water at the $CH_2Cl_2-H_2O$ interface. This is consistent with the featureless spectral response previously observed for water at the DCE−$H_2O$ interface.[8]

Overall, these spectral profiles show the free OH mode produces a sum frequency signal only within the interfacial region, despite possessing population within the bulk water

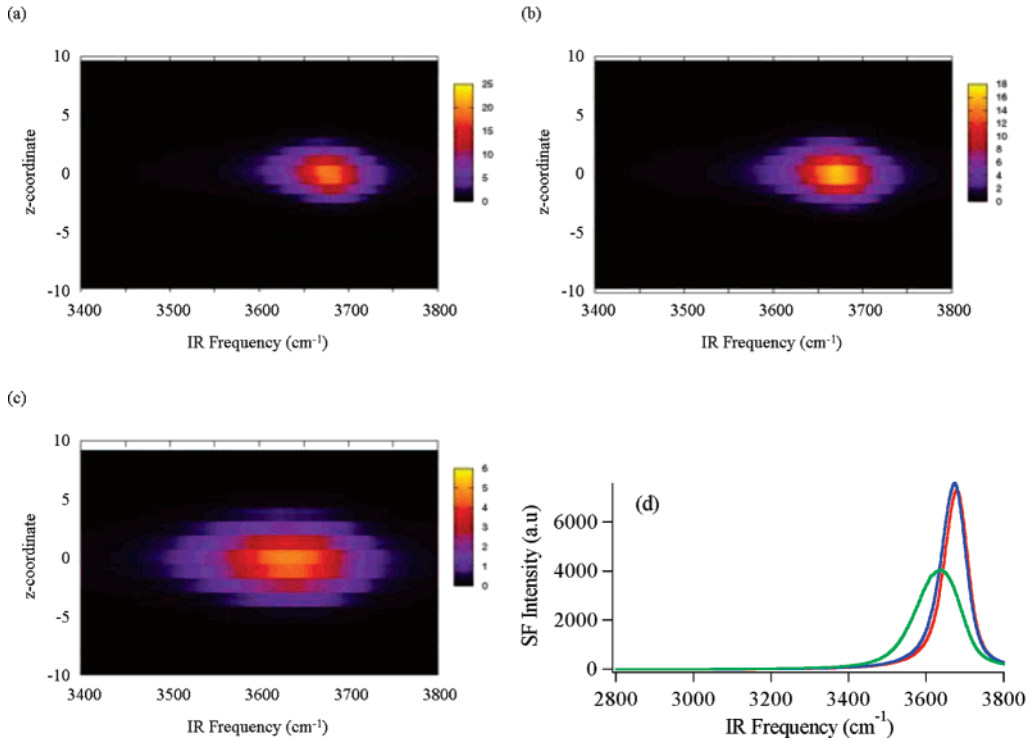


**Figure 3.** Sum frequency spectral profiles of the free OH mode from straddling water molecules at the (a) $CCl_4-H_2O$ interface, (b) $CHCl_3-H_2O$ interface, and (c) $CH_2Cl_2-H_2O$ interface. (d) Sum frequency spectral intensities of the free OH mode at the $CCl_4-H_2O$ (red), $CHCl_3-H_2O$ (blue), and $CH_2Cl_2-H_2O$ (green) interfaces. All spectra are shown in SSP polarization and possess bin sizes of 1 Å and/or 1 $cm^{-1}$.

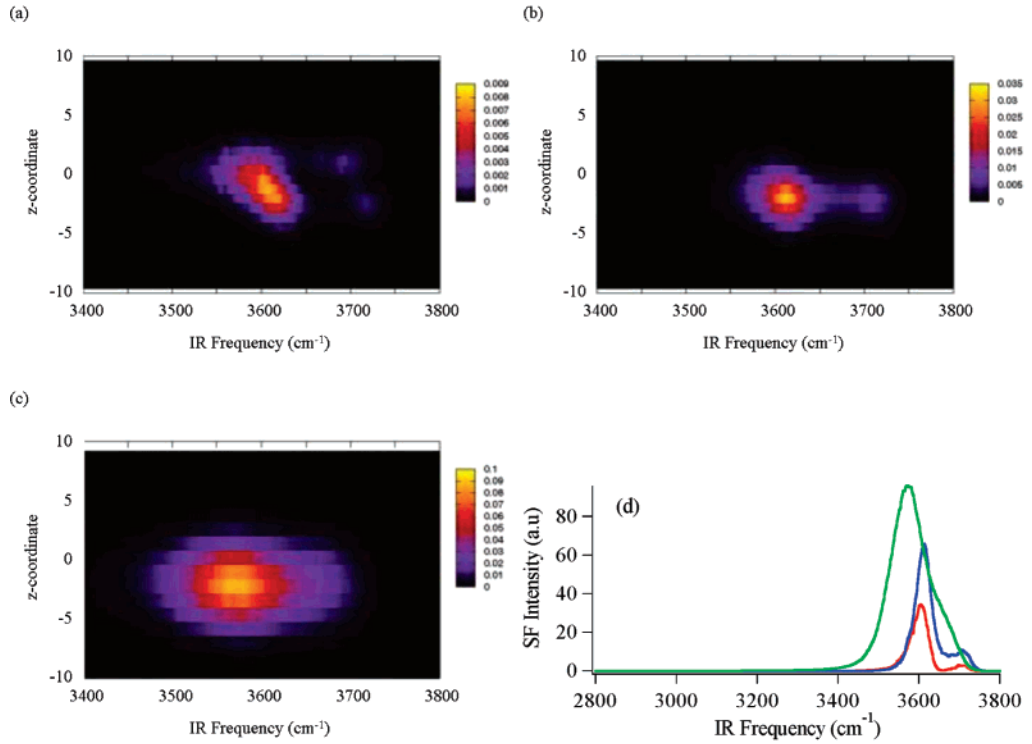


**Figure 4.** Sum frequency spectral profiles of hydrogen bond acceptors at the (a) $CCl_4-H_2O$ interface, (b) $CHCl_3-H_2O$ interface, and (c) $CH_2Cl_2-H_2O$ interface. (d) Sum frequency spectral intensities of hydrogen bond acceptors at the $CCl_4-H_2O$ (red, ×10), $CHCl_3-H_2O$ (blue, ×5), and $CH_2Cl_2-H_2O$ (green) interfaces. All spectra are shown in SSP polarization and possess bin sizes of 1 Å and/or 1 $cm^{-1}$.

phase (see Figure 1b). This is not surprising, as bulk water molecules are randomly oriented and do not produce a net sum frequency response under the dipole approximation. These results clearly emphasize the differences between molecular population and molecular orientation for this species of water and justify the notion that straddling water molecules "exist" only at the interface.

The depth profiling of hydrogen bond acceptors provide additional insights into the different degrees of water penetration and orientation at these interfaces. Figures 4a through 4c show sum frequency spectral depth profiles of hydrogen bond acceptors at the $CCl_4-H_2O$, $CHCl_3-H_2O$, and $CH_2Cl_2-H_2O$ interfaces, respectively. Figure 4d shows their corresponding sum frequency intensities. All spectra are shown in SSP

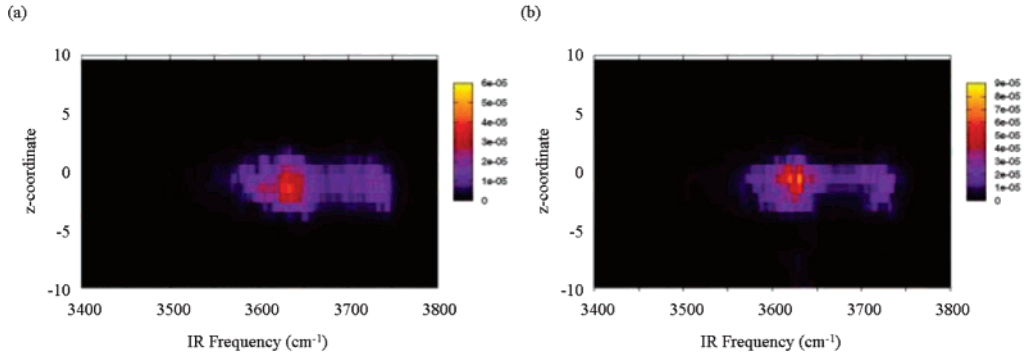


**Figure 5.** Sum frequency spectral profiles of water monomers at the (a) $CCl_4-H_2O$ interface and (b) $CHCl_3-H_2O$ interface. All spectra are shown in SSP polarization and possess bin sizes of 1 Å and 1 $cm^{-1}$.

polarization. The OH oscillators from hydrogen bond acceptors are in similar environments causing them to be energetically coupled enough to produce clear symmetric and antisymmetric OH stretch modes. If one looks at Figure 4d for the $CCl_4-H_2O$ interface, both the symmetric and antisymmetric modes are clearly present in the calculated spectral response from hydrogen bond acceptors. These two peaks are also apparent in the depth profile spectra (Figure 4a). The dominant region of spectral intensity at lower frequencies is attributed to the symmetric OH stretch mode, while the lesser regions of spectral intensity at higher frequencies are attributed to the antisymmetric OH stretch mode. Of note, as a function of interfacial depth, these spectral features shift toward higher frequencies when progressing across the interface from the $H_2O$ phase to the $CCl_4$ phase. We attribute this spectral shift to the identification of hydrogen bond acceptors that possess different degrees of hydrogen bonds to their oxygen atoms: water molecules possessing two intermolecular hydrogen bonds would be expected to reside closer to the water phase (lower frequencies) while molecules possessing one intermolecular hydrogen bond (higher frequencies) reside closer to the $CCl_4$ phase.[36]

For the $CHCl_3-H_2O$ interface the sum frequency spectral depth profile of hydrogen bond acceptors (Figure 4b) also shows distinct contributions from symmetric and antisymmetric OH stretch modes. This is also apparent in the calculated spectral contributions (Figure 4d). However, for this system there is no clear spectral shift as these water molecules move across the interface as was seen for the $CCl_4-H_2O$ interface. It is also worth noting that the peak signal from hydrogen bond acceptors at the $CHCl_3-H_2O$ interface is approximately four times greater than the overall peak signal of the corresponding profile at the $CCl_4-H_2O$ interface (Figure 4d), along with a narrow distribution of bonding interactions across the interface. It is somewhat surprising that the interfacial width of this profile is narrower than the interfacial width of the corresponding profile at the $CCl_4-H_2O$ interface; this is not apparent from their density profiles (see Figure 1c).

Interestingly, for the $CH_2Cl_2-H_2O$ interface, Figures 4c and 4d show less distinct features for the symmetric and antisymmetric stretch modes from hydrogen bond acceptors. The spectral depth profile (Figure 4c) shows a relatively broad response in both frequency and interfacial depth. It has an overall frequency shift to energies lower than that found in the previous two interfacial systems. Following an asymmetric line shape, the spectral peak intensity at lower frequencies is consistent with the symmetric OH stretch mode, followed by a shoulder of intensity at higher frequencies that likely corresponds to the antisymmetric OH stretch mode. An additional important observation is that for the $CH_2Cl_2-H_2O$ interface there is a significant increase in penetration of water into the $CH_2Cl_2$ phase. In all three of these liquid−liquid systems, hydrogen bond acceptors produce the majority of their spectral response within the organic phase. This is emphasized to a significant degree by hydrogen bond acceptors at the $CH_2Cl_2-H_2O$ interface.

Figure 4d shows the corresponding sum frequency intensities from hydrogen bond acceptors at each liquid−liquid interface. The spectral intensities from hydrogen bond acceptors at the $CCl_4-H_2O$ and $CHCl_3-H_2O$ interfaces are scaled by factors of $\times 10$ and $\times 5$, respectively, to fit the graph. (Intensities are not scaled in the corresponding spectral profiles of these systems.) A comparison of these calculated spectral intensities shows that the spectral intensity from hydrogen bond acceptors at the $CH_2Cl_2-H_2O$ interface is much greater than that observed even at the $CHCl_3-H_2O$ interface. This implies that the spectral contribution from hydrogen bond acceptors will play a much larger role within the $CH_2Cl_2-H_2O$ interfacial system compared to the other interfacial systems. These observations are attributed to a broad range and large number of $CH_2Cl_2-H_2O$ bonding interactions within that interfacial region.

The relatively large contribution and spectral breadth displayed by hydrogen bond acceptors at the $CH_2Cl_2-H_2O$ interface indicates that these modes play a large role in the overall VSF spectrum generated from this interface. Interferences in the modes present in the high-frequency portion of the $CH_2Cl_2-H_2O$ spectral region largely dictate its shape and distinct spectral characteristics. The large spectral contribution from hydrogen bond acceptors coincides with VSF experimental studies of the DCE−$H_2O$ interface and ($CCl_4$ + $CH_2Cl_2$)−$H_2O$ interface studies where a nearly featureless sum frequency spectral response from water is observed.[8,35] At the $CH_2Cl_2-H_2O$ interface, the phase of the spectral response from the free OH mode constructively interferes with the phase from hydrogen bond acceptors at lower frequencies (where the symmetric OH stretch mode predominates) and destructively interferes with the phase from hydrogen bond acceptors at higher frequencies (where the antisymmetric OH stretch mode predominates). This results in an accumulation of sum frequency intensity on the lower frequency side of the free OH peak and a reduction of sum frequency intensity on the higher frequency side of the free OH peak. As a consequence, there is a loss in a distinct free OH peak within the overall spectrum (see Figure 2d).[8]

Interfacial water monomers, or water molecules that have no bonding to other water molecules, are also present with differing characteristics and with different degrees of impact on the VSF spectra for these three systems. Figures 5a and 5b show sum frequency spectral depth profiles of water monomers at the $CCl_4-H_2O$ and $CHCl_3-H_2O$ interfaces, respectively. Figure 5a shows the sum frequency spectral depth profile of water monomers at the $CCl_4-H_2O$ interface is spatially localized within the interfacial region with the highest population in the

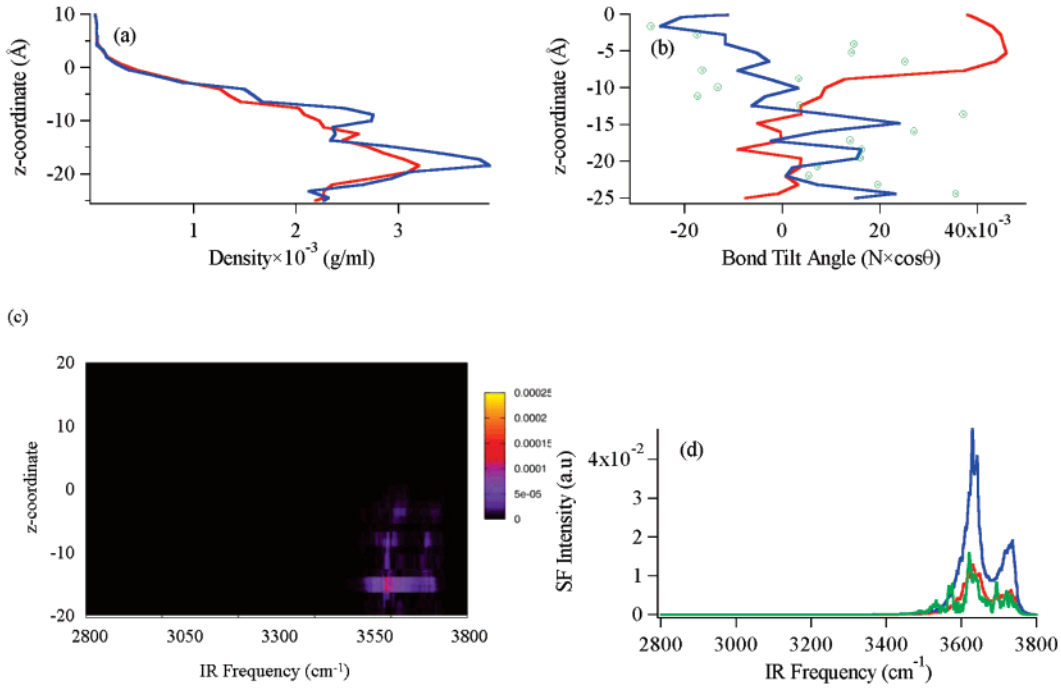


**Figure 6.** (a) Density profile of water monomers at the $CH_2Cl_2-H_2O$ interface after 1 ns (blue) and 3 ns (red). (b) Tilt angle distributions of OH bonds from hydrogen bond acceptors (red) and water monomers (blue) at the $CH_2Cl_2-H_2O$ interface after 3 ns. Also shown are data points (green) representing the tilt angle distribution of OH bonds from water monomers after 1 ns. The two tilt angle distributions of OH bonds from water monomers are scaled equally (×5) to fit the graph. (c) Sum frequency spectral profile of water monomers at the $CH_2Cl_2-H_2O$ interface after 3 ns. (d) Sum frequency spectral intensities of water monomers at the $CCl_4-H_2O$ (red), $CHCl_3-H_2O$ (blue), and $CH_2Cl_2-H_2O$ (green) interfaces after 3 ns. All spectra are shown in SSP polarization and possess bin sizes of 1 Å and/or 1 $cm^{-1}$.

organic rich region of the interface. As is observed with hydrogen bond acceptors at this interface, the OH oscillators from water monomers reside in similar environments and produce clear symmetric and antisymmetric OH stretch modes. The symmetric OH stretch mode appears as a peak of high intensity at lower frequencies, and the antisymmetric OH stretch mode appears as a tail of lower spectral intensity at higher frequencies.

Figure 5b shows that the sum frequency spectral depth profile of oriented water monomers at the $CHCl_3-H_2O$ interface is also localized within the interfacial region, producing clear symmetric and antisymmetric OH stretch modes at lower and higher frequencies, respectively. Density profiles of water monomers within this system show that the population of water monomers (not necessarily oriented) persists throughout much of the $CHCl_3$ phase, and this population is greater at all depths when compared to the population of water monomers at the $CCl_4-H_2O$ interface. As a result, one might expect a higher sum frequency spectral response from water monomers at the $CHCl_3-H_2O$ interface compared to the $CCl_4-H_2O$ interface merely due to the higher concentration of water molecules in the former; this observation is consistent with the spectral responses calculated in the depth profiles of water monomers from these systems.

The distribution of water monomers at the $CH_2Cl_2-H_2O$ interface warrants close scrutiny, as Figure 1d shows a small but significant density at least 10 Å into the organic phase. Presenting a view extending deeper into the $CH_2Cl_2$ phase, Figure 6a reveals a peak population from water monomers of approximately $3 \times 10^{-3}$ g/mL, residing approximately 17 Å into the $CH_2Cl_2$ phase. This peak population appears after 1 ns of simulation time (20 000 configurations) and persists through 3 ns of simulation time (60 000 configurations). This persistence in density indicates an equilibrated and stable population of water monomers in the $CH_2Cl_2$ phase.

Figure 6b shows the tilt angle distribution of the OH bonds from water monomers and hydrogen bond acceptors at the $CH_2Cl_2-H_2O$ interface. In this graph, the vertical axis represents the *z*-coordinate and the horizontal axis represents the OH bond tilt angle. Positive values of the tilt angle represent water molecules with their OH oscillators directed toward the $CH_2Cl_2$ phase, while negative values represent water molecules with their OH oscillators directed toward the $H_2O$ phase. Figure 6b shows that hydrogen bond acceptors direct their OH oscillators toward the $CH_2Cl_2$ phase. This is to be expected, as these molecules possess intermolecular hydrogen bonds incident only upon their oxygen atoms. The preferential orientation of water monomers however is a little more complex. Water monomers closest to the Gibbs surface generally prefer to direct their OH oscillators toward $H_2O$, while monomers further away from the Gibbs surface prefer to direct their OH oscillators toward $CH_2Cl_2$. This response appears quite noisy after only 1 ns of simulation time but is readily apparent after 3 ns of simulation time. This tilt angle distribution reveals two separate regions of oppositely oriented water monomers, which has also been observed in calculations at the $DCE-H_2O$ interface.[36]

Figure 6c shows that the sum frequency spectral profile of water monomers at the $CH_2Cl_2-H_2O$ interface produces no significant response immediately at the Gibbs surface. Much of the spectral response from water monomers appears more than several angstroms away from the Gibbs surface, inside the bulk $CH_2Cl_2$ phase, indicating that these water monomers are still oriented (as is also shown in Figure 6b). The presence of distinguishable symmetric and antisymmetric OH stretch modes is vague, and each OH stretch mode broadens as a function of depth within the $CH_2Cl_2$ phase, indicating a broader distribution of $H_2O-CH_2Cl_2$ interactions. The largest spectral response appears near the peak population of water monomers in the $CH_2Cl_2$ phase, approximately 15 Å away from the Gibbs surface.

But despite this large population when compared to water monomers in other systems, the integration of sum frequency signal within the spectral depth profile of Figure 6c does not result in a large sum frequency spectral intensity, as is shown in Figure 6d. The sum frequency intensity of water monomers at the $CH_2Cl_2-H_2O$ interface is only of similar magnitude with respect to the sum frequency intensity of water monomers at the $CCl_4-H_2O$ interface. This can be attributed to the destructive interference between water molecules in the $CH_2Cl_2-H_2O$ system that have different orientations as a function of depth.

The orientation distribution of water monomers can be understood by considering a polarization generated by the water surface that emits an electric field, normal to the surface, into the adjacent phase. The surface polarization generated by water has been studied in some detail.[33,37] With respect to these studies, the polarization can be attributed largely to hydrogen bond acceptors, as these molecules are optimally oriented with their dipole moments perpendicular to the water surface. Considering the electric field emitted by hydrogen bond acceptors on a local, molecular scale (as is described by Ishiyama and Morita for water molecules at the vapor−water interface[38]), water monomers located within the same spatial region as hydrogen bond acceptors (approximately $0\ \text{Å} < z < -10\ \text{Å}$) will be oriented opposite to hydrogen bond acceptors, due to the local propagation of the electric field. Conversely, water monomers located further away from the spatial region occupied by hydrogen bond acceptors (approximately $-10\ \text{Å} < z < -20\ \text{Å}$) will be oriented in the same direction as hydrogen bond acceptors, due to the extended propagation of the electric field away from the surface. This latter case will only be observed by interfacial systems that produce large quantities of water monomers, as is shown for the $CH_2Cl_2-H_2O$ and $DCE-H_2O$[36] interfaces. In these interfacial systems, water monomers produce two separate spatial regions of oppositely oriented molecules. For the $CHCl_3-H_2O$ and $CCl_4-H_2O$ interfacial systems, only the spatial region located closest to the surface will be occupied by water monomers due to reduced solubility. Generally, water monomers in these systems produce clear tilt angle preferences with their OH oscillators directed toward the $H_2O$ phase, resulting in greater sum frequency intensities.

## Conclusions

Molecular dynamics simulations are performed to generate density profiles, sum frequency spectral intensities, and sum frequency spectral profiles of water at the $CCl_4-H_2O$ interface, the $CHCl_3-H_2O$ interface, and the $CH_2Cl_2-H_2O$ interface. In each of these systems, focus is placed upon the molecular composition and orientation of interfacial water, in addition to several species of water that interact directly with the organic phases. Density profiles are used to determine their molecular populations as a function of interfacial depth, while sum frequency intensities are used to determine their spectral responses as a function of OH vibrational frequency. Sum frequency spectral profiles are used to determine their spectral responses as functions of both OH vibrational frequency and interfacial depth. These spectral profiles provide a visual means of correlating the molecular population and orientation of different species of water in a manner that can be difficult to provide from density profiles and sum frequency spectral intensities.

The results of these calculations highlight the differences in water structure within these interfacial systems. In general, interfacial widths of these liquid−liquid systems coincide with the polarity of the organic liquid, with the $CH_2Cl_2-H_2O$ interfacial width being the largest and the $CCl_4-H_2O$ interfacial width being the smallest. This trend is observed with both density profiles and spectral profiles. Following this trend that relates to the polarity of the organic liquid, free OH modes from straddling water molecules exhibit varying degrees of interaction with the organic phase, where the $H_2O-CH_2Cl_2$ interaction is the strongest and the $H_2O-CCl_4$ interaction is the weakest. This is observed with both sum frequency spectral intensities and spectral profiles. Hydrogen bond acceptors generally reveal clear symmetric and antisymmetric OH stretch modes, and the spatial resolution of molecules possessing one versus two intermolecular hydrogen bonds on the oxygen atom is observed with spectral profiles at the $CCl_4-H_2O$ interface. Spectral profiles are also used to show that water monomers are oriented deep within the $CH_2Cl_2$ phase and that these penetrating water molecules possess varying orientations throughout the organic rich region of the interface.

Vibrational sum frequency spectroscopy is a proven method for the study of water surfaces. Over the past several years, many intriguing computational approaches have been taken toward the calculation of sum frequency spectra and have been targeted primarily toward experimental measurements of vapor−water interfacial systems.[27,38−46] This computational approach is extending our understanding of water at these complex liquid−liquid interfaces by creating a unique visual tool capable of discerning intimate details involving water structure, bonding, and penetration within buried interfacial systems.

**Acknowledgment.** We thank the National Science Foundation (Grant CHE 0652531) and the Office of Naval Research for supporting this study.

## References and Notes

(1) Brown, M. G.; Walker, D. S.; Raymond, E. A.; Richmond, G. L. *J. Phys. Chem. B* **2003**, *107*, 237.
(2) Du, Q.; Freysz, E.; Shen, Y. R. *Science* **1994**, *264*, 826.
(3) Leich, M. A.; Richmond, G. L. *Faraday Discuss.* **2005**, *129*, 1.
(4) Richmond, G. L. *Chem. Rev.* **2002**, *102*, 2693.
(5) Scatena, L. F.; Richmond, G. L. *J. Phys. Chem. B* **2001**, *105*, 11240.
(6) Scatena, L. F.; Richmond, G. L. *J. Phys. Chem. B* **2004**, *108*, 12518.
(7) Walker, D. S.; Brown, M. G.; McFearin, C. L.; Richmond, G. L. *J. Phys. Chem. B* **2004**, *108*, 2111.
(8) Walker, D. S.; Moore, F. G.; Richmond, G. L. *J. Phys. Chem. C* **2007**, *111*, 6103.
(9) Watry, M. R.; Richmond, G. L. *Langmuir* **2002**, *18*, 8881.
(10) Watry, M. R.; Richmond, G. L. *J. Phys. Chem. B* **2002**, *106*, 12517.
(11) Mitrinovic, D. M.; Zhang, Z.; Williams, S. M.; Huang, Z.; Schlossman, M. L. *J. Phys. Chem. B* **1999**, *103*, 1779.
(12) Schlossman, M. L. *Curr. Opin. Colloid Interface Sci.* **2002**, *7*, 235.
(13) Tikhonov, A. M.; Mitrinovic, D. M.; Li, M.; Huang, Z.; Schlossman, M. L. *J. Phys. Chem. B* **2000**, *104*, 6336.
(14) Teixeira, J.; Bellisent-Funel, M. C. *J. Phys.: Condens. Matter* **1990**, *2*.
(15) Strutwolf, J.; Barker, A. L.; Gonsalves, M.; Caruana, D. J.; Unwin, P. R.; Williams, D. E.; Webster, J. R. P. *J. Electroanal. Chem.* **2000**, *483*, 163.
(16) Steel, W. H.; Walker, R. A. *J. Am. Chem. Soc.* **2003**, *125*, 1132.
(17) Steel, W. H.; Lau, Y. Y.; Beildeck, C. L.; Walker, R. A. *J. Phys. Chem. B* **2004**, *108*, 13370.
(18) Benjamin, I. *J. Chem. Phys.* **1992**, *97*, 1432.
(19) Benjamin, I. *J. Phys. Chem. B* **2005**, *109*, 13711.
(20) Dang, L. X. *J. Phys. Chem. B* **2001**, *105*, 804.
(21) Pratt, L.; Pohorille, A. *Chem. Rev.* **2002**, *102*, 2671.
(22) Senapati, S.; Berkowitz, M. L. *Phys. Rev. Lett.* **2001**, *87*, 176101.
(23) Case, D. A.; Pearlman, D. A.; Caldwell, J. W.; Cheatham, T. E., III; Wang, J.; Ross, W. S.; Simmerling, C. L.; Darden, T. A.; Merz, K. M.; Stanton, R. V.; Cheng, A. L.; Vincent, J. J.; Crowley, M.; Tsui, V.; Gohlke, H.; Radmer, R. J.; Duan, Y.; Pitera, J.; Massova, I.; Seibel, G. L.; Singh, U. C.; Weiner, P. K.; Kollman, P. A. *AMBER 7*; University of California: San Francisco, CA, 2002.

(24) Caldwell, J. W.; Kollman, P. A. *J. Phys. Chem.* **1995**, *99*, 6208.
(25) Chang, T. M.; Peterson, K. A.; Dang, L. X. *J. Chem. Phys.* **1995**, *103*, 7502.
(26) Chang, T. M.; Dang, L. X.; Peterson, K. A. *J. Phys. Chem. B* **1997**, *101*, 3413.
(27) Morita, A.; Hynes, J. T. *Chem. Phys.* **2000**, *258*, 371.
(28) Walker, D. S.; Hore, D. K.; Richmond, G. L. *J. Phys. Chem. B* **2006**, *110*, 20451.
(29) McFearin, C. L.; Moore, F. G.; Hore, D. K.; Richmond, G. L. *J. Phys. Chem. C*, manuscript in preparation.
(30) Raymond, E. A.; Tarbuck, T. L.; Brown, M. G.; Richmond, G. L. *J. Phys. Chem. B* **2003**, *107*, 546.
(31) Walker, D. S.; Richmond, G. L. *J. Phys. Chem. C* **2007**, in press.
(32) Hore, D. K.; Walker, D. S.; Richmond, G. L. *J. Am. Chem. Soc.* **2006**, *129*, 752.
(33) Hore, D. K.; Walker, D. S.; MacKinnon, L.; Richmond, G. L. *J. Phys. Chem. C* **2007**, *111*, 752.
(34) Moller, K. B.; Rey, R.; Hynes, J. T. *J. Phys. Chem. A* **2004**, *108*, 1275.
(35) McFearin, C. L.; Richmond, G. L. *J. Mol. Liq.* **2007**, *136*, 221.
(36) Walker, D. S.; Richmond, G. L. *J. Am. Chem. Soc.* **2007**, *129*, 9446.
(37) Chang, T. M.; Dang, L. X. *J. Chem. Phys.* **1996**, *104*, 6772.
(38) Ishiyama, T.; Morita, A. *J. Phys. Chem. C* **2007**, *111*, 738.
(39) Benjamin, I. *Phys. Rev. Lett.* **1994**, *73*, 2083.
(40) Buch, V. *J. Phys. Chem. B* **2005**, *109*, 17771.
(41) Ishiyama, T.; Morita, A. *J. Phys. Chem. C* **2007**, *111*, 721.
(42) Morita, A.; Hynes, J. T. *J. Phys. Chem. B* **2002**, *106*, 673.
(43) Morita, A. *J. Phys. Chem. B* **2006**, *110*, 3158.
(44) Perry, A.; Ahlborn, H.; Space, B. *J. Chem. Phys.* **2003**, *118*, 8411.
(45) Perry, A.; Neipert, C.; Kasprzyk, C. R.; Green, T.; Space, B. *J. Chem. Phys.* **2005**, *123*, 11.
(46) Perry, A.; Neipert, C.; Ridley, C.; Space, B. *Phys. Rev. E* **2005**, *71*, 4.